Chapter 6
Electrical Conductivity and ^{7}Li NMR Spin-Lattice Relaxation in Amorphous, Nano- and Microcrystalline Li_2O-7GeO_2

O. Nesterov, M. Trubitsyn, O. Petrov, M. Vogel, M. Volnianskii, M. Koptiev, S. Nedilko, and Ya. Rybak

6.1 Introduction

Applications in modern electronics and power engineering stimulate active studies of ionic conduction in dielectric solids [1, 2]. As a rule, the structures of ionic conductors contain a large number of vacant positions which can be occupied by mobile ions. Besides vacant positions should be separated by not too high potential barriers and connected by channels that enable ionic migration through the lattice framework. Such structural features provide for fast ionic conduction at moderate temperatures. The crystals of the lithium germanate family are considered as perspective matrixes to create new materials with high ionic conductivity. By now, about ten representatives of the Li_2O-GeO_2 family have been synthesized [3], and special attention is devoted to the ferroelectric crystals of lithium tetragermanate ($Li_2Ge_4O_9$) and lithium heptagermanate ($Li_2Ge_7O_{15}$) which are typical dielectrics with an energy gap of about 5 eV width [4]. The structures of these crystals have framework type and are formed by germanium-oxygen octahedra [GeO_6] and tetrahedra [GeO_4], which are connected by polyhedral edges or by bridging oxygen atoms [5–7]. The Li^+ ions are located within the cavities, formed by the germanium-oxygen structural skeleton. Electrical conductivity in pure and 3d-ion-

O. Nesterov · M. Trubitsyn (✉) · M. Volnianskii · M. Koptiev
Solid State Physics and Optoelectronics Department, Oles Honchar Dnipro National University, Dnipro, Ukraine

O. Petrov · M. Vogel
Institute of Solid State Physics, Darmstadt Technical University, Darmstadt, Germany
e-mail: michael.vogel@physik.tu-darmstadt.de

S. Nedilko · Ya. Rybak
Physics Faculty, Taras Shevchenko National University of Kyiv, Kyiv, Ukraine
e-mail: snedilko@univ.kiev.ua

O. Fesenko, L. Yatsenko (eds.), *Nanocomposites, Nanostructures, and Their Applications*, Springer Proceedings in Physics 221,
https://doi.org/10.1007/978-3-030-17759-1_6

doped $Li_2Ge_7O_{15}$ crystals was studied in previous works [8–12]. It was shown that charge transfer was determined by Li^+ interstitial ions hopping through the channels of the $Li_2Ge_7O_{15}$ structure [10–12].

Today nanostructuring is actively used to create dielectrics with a high ionic component of the electrical conductivity. Reducing the size of structural inhomogeneities down to the nanometer range makes it possible to increase ionic conductance and even to induce a transition to a superionic phase [1, 2]. Spatially heterogeneous solid electrolytes, which consist of more than one phase, are of particular interest. The relative volume of the phases and size of the homogeneous regions as well as their spatial distribution become the essential factors for such materials. One of the effective ways to obtain nanostructured materials is heat treatment and partial crystallization of initial amorphous phases. It is known that the maximal increase of the number of crystal nuclei and the maximal growth of the size of the nuclei occur at different temperatures. Thus, selecting the regimes of glass heat treatment allows one to control the mean size of nanoregions, enabling a preparation of highly dispersed states which have the same chemical composition as the homogeneous medium, but significantly different properties. Varying stoichiometry and temperature regimes of glass devitrification, one can control chemical composition, structure and morphology of ordered and interfacial regions.

Recently the preparation of Li_2O-$x$$GeO_2$ glasses and their crystallization on heating were studied in [13–17]. It was shown that amorphous phases crystallized in stages depending on the proportion x of the starting reagents. In this paper, we study electrical properties (conductivity σ and complex impedance ρ*) of the states obtained from crystallization of Li_2O-$7GeO_2$ glass. In order to determine the mechanisms of charge transfer, the ^{7}Li NMR spin-lattice relaxation (SLR) rate was measured in Li_2O-$7GeO_2$ glass, intermediate nanocrystalline state and polycrystal. The NMR SLR data are compared with the results of conductivity and complex impedance studies.

6.2 Experimental Details

Lithium heptagermanate Li_2O-$7GeO_2$ glass was prepared by fast quenching of the melt. In general, Li_2O-$x$$GeO_2$ glasses can be crystallized by heating or by isothermal heat treatment [17, 18]. Here we devitrified Li_2O-$7GeO_2$ glass only on heating. The temperatures characterizing glass devitrification were determined by differential scanning calorimetry (DSC) (Mettler STARe SW derivatograph). The structure and morphology of the heterogeneous states, obtained at glass crystallization, were studied by X-ray phase analysis (DRON-3) and atomic force microscopy (AFM) (Integra Prima Basic NT-MDT microscope) [19, 20]. Electrical properties were measured in an AC field by using a bridge method (AC bridges E7-10, Tesla BM-507). ^{7}Li NMR spin-lattice relaxation measurements were performed at a Larmor frequency of 139.9 MHz using a saturation-recovery sequence in combination with

solid-echo detection. Further details of the ^{7}Li NMR experimental setup can be found in previous work [21].

6.3 Results and Discussion

6.3.1 *Structure and Morphology of the States Resulting from Glass Devitrification*

Crystallization of the Li_2O-$7GeO_2$ glass was studied by DSC. The data obtained were consistent with previous results for the Li_2O-$xGeO_2$ family [13–17]. The DSC thermogram (Fig. 6.1) showed a weak anomaly at the glass transition temperature T_g and two exothermic peaks, indicating stepwise crystallization of the amorphous phase. The DSC anomalies were detected only during the first heating run of the original glass, while they were absent during subsequent temperature cycling as a result of the preceding complete glass crystallization.

Phase compositions of the states appearing at glass crystallization were investigated by X-ray phase analysis (Fig. 6.2) [19]. The samples in the intermediate state were prepared by heating the glass to temperatures between the first and the second DSC peaks ($T_1 < T < T_2$) and subsequent cooling to room temperature. The polycrystalline samples were obtained by heating the glass to temperatures above the second DSC peak ($T > T_2$) and subsequent cooling to room temperature.

It was concluded that the first DSC peak is associated with an appearance of nuclei of lithium tetragermanate $Li_2Ge_4O_9$ and lithium heptagermanate $Li_2Ge_7O_{15}$ phases. Heating above T_2 led to complete crystallization of the thermodynamically stable $Li_2Ge_7O_{15}$ phase. The lithium tetragermanate phase disappeared and transformed to the lithium heptagermanate one in accord with $Li_2Ge_4O_9 + 3GeO_2 \rightarrow Li_2Ge_7O_{15}$. As it was discussed in [7], transformation of $Li_2Ge_4O_9$ nuclei into $Li_2Ge_7O_{15}$ ones was possible, because lithium tetragermanate

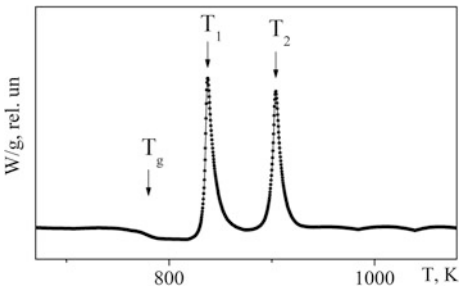

Fig. 6.1 DSC thermogram measured on heating the original Li_2O-$7GeO_2$ glass. Three anomalies were detected: inflection at the glass transition point $T_g = 775$ K and two exothermic peaks at $T_1 = 838$ K and $T_2 = 904$ K. Temperature was increased with a rate of 10 K/min

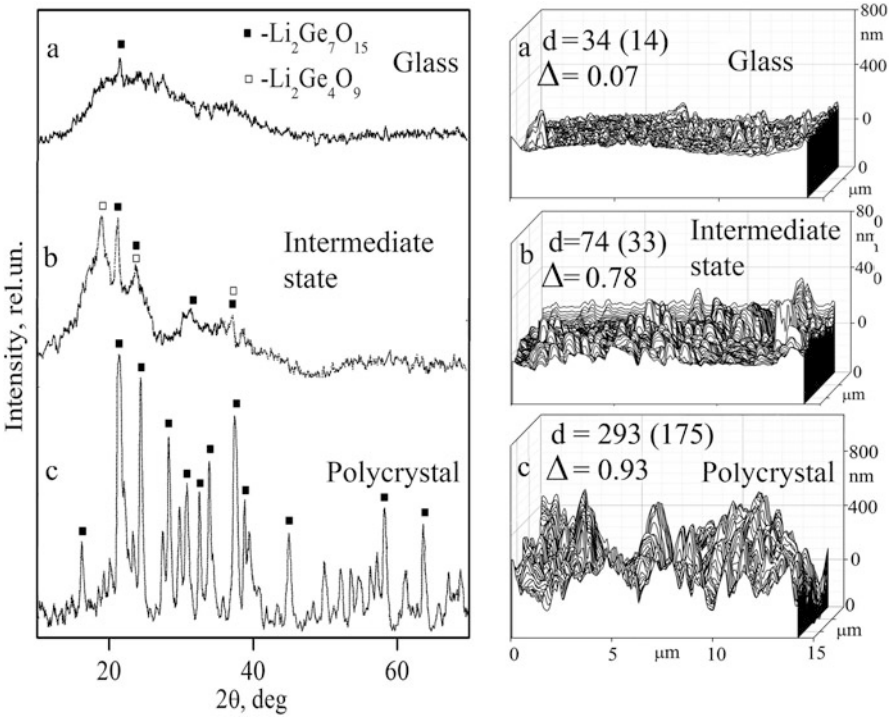

Fig. 6.2 X-Ray diffraction patterns (on the left) and profiles of AFM images (on the right) for the states formed during Li_2O-7GeO_2 glass crystallization: glass (**a**), intermediate state (**b**) and polycrystal (**c**) [19, 20]. Average linear size d of the ordered regions (in nm) and ordered phase fraction Δ are indicated on the AFM images

and lithium heptagermanate have similar crystal structures formed by octahedral and tetrahedral germanium-oxygen polyhedra.

The morphology of the states obtained at glass devitrification was studied by AFM [20]. Figure 6.2 shows the profiles of AFM images. Moreover, the mean linear size d of the ordered nuclei and the relative fraction Δ of the ordered regions are indicated. One can see that in the intermediate state, the ordered phases with nanometer-sized nuclei ($d = 74$ nm) occupy about three quarters of the sample volume, whereas amorphous surroundings occupy the rest one quarter. In the polycrystalline samples, the crystallites with micrometer-ranged average size ($d \approx 0.3$ μm) occupy nearly the whole sample volume.

6.3.2 Electrical Conductivity

Preliminary data of the conductivity σ of Li_2O-7GeO_2 as-quenched glass were presented in the previous work [20]. The results were obtained during the first heating run up to temperatures in the interval between T_1 and T_2 of DSC anomalies (Fig. 6.1). It was shown that σ sufficiently increased in the intermediate nanocrystalline state. Nevertheless, for the nonstoichiometric composition Li_2O-11.5GeO_2 [18], it was demonstrated that the glass could be completely crystallized not only by heating over T_2 but also by isothermal heat treatment at a temperature in the interval between T_g and T_1. This means that the intermediate nanocrystalline state is in fact metastable. It is of interest to clarify the conditions which allow one to stabilize such nanostructured state with increased conductivity. Therefore, in this study, we used the following temperature cycles. At first, the as-quenched glass was heated up to a temperature of T_g – 100 K and then cooled to room temperature. The upper limit in this cycle was chosen to avoid changes of the amorphous state of the sample during the measurements. Next the sample was heated up to T_1 + 9 K, transformed to the intermediate nanocrystalline state and immediately after that cooled to room temperature. Finally the sample was heated over the second DSC peak up to T_2 + 27 K, underwent complete crystallization and subsequently cooled to room temperature. The heating and cooling rates were 3.3 K/min. The conductivity σ was measured in an AC field (f = 1 kHz) during the above-described temperature runs.

Figure 6.3 shows the results in an Arrhenius plot. One can see that a nearly linear behavior of $\sigma(1/T)$ observed for the glass is changed to a steeper increase when heating through T_g as a result of glass softening. In the range between T_1 and T_2, the conductivity of the sample significantly increases until it eventually drops sharply on crossing T_2.

According to [9–12], charge transfer in single crystalline $Li_2Ge_7O_{15}$ is determined by Li^+ interstitials hopping along the structural channels. Thus, the increase of σ with temperature is governed by thermal activation of the charge carrier's mobility. Based on this data, one can assume that the conductivities of Li_2O-7GeO_2 glass, intermediate nanocrystalline state and polycrystal are determined by Li^+ ions which are mobile enough owing to weak bonds with germanium-oxygen structural framework [6].

A thermally activated increase of the conductivity is usually described by the expression

$$\sigma(T) = \frac{A}{T} \exp\left(-E_\sigma \Big/ k_B T\right), \tag{6.1}$$

where E_σ is the activation energy of conductivity; k_B the Boltzmann constant, $A = nq^2\delta^2\nu/(zk_B)$; n, q and δ the carrier's concentration, charge and hopping length, respectively; ν the frequency of lattice vibrations; and z the number of nearest available positions. The values of the parameters in Eq. 6.1 obtained for the studied states are presented in Table 6.1. One can see that at 500 K conductivity of the

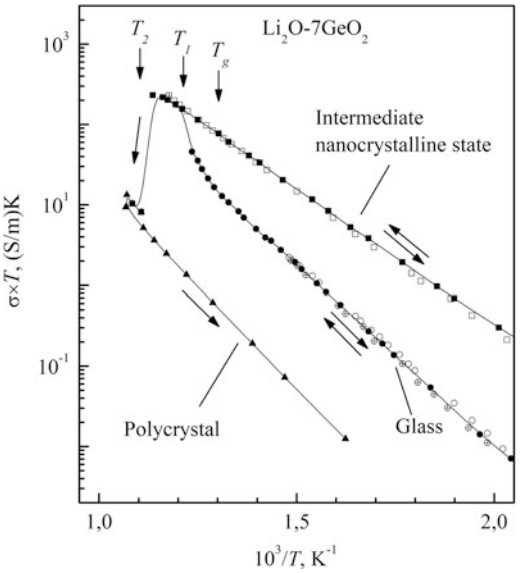

Fig. 6.3 Conductivity of Li_2O-7GeO_2 states vs. $1/T$. Measurements were carried out in an AC field ($f = 1$ kHz) by using the temperature regimes described in the text. The temperatures of DSC anomalies (Fig. 6.1) are shown by arrows

Table 6.1 Conductivity and values of the parameters in Eq. 6.1 determined from the linear regions in the Arrhenius plot shown in Fig. 6.3

Li_2O-7GeO_2 states	Conductivity σ, S/m, ($T = 500$ K)	Factor A, $\times 10^5$, (S/m)·K	Activation energy, eV	
			E_σ	E_{SLR}
Glass	2.4×10^{-5}	100 (30)	0.89 (2)	0.45(1)
Intermediate nanocrystalline state	4.8×10^{-4}	25(5)	0.69(1)	0.26(1)
Polycrystal	~1.6×10^{-6}	24(5)	1.01(1)	0.58(3)

The right column shows the values of the activation energy determined from NMR SLR data (Sec. 6.3.4)

nanocrystalline state is one order higher than for the glass and two orders higher than for the polycrystal grained in the micrometer range. Consistently the E_σ has the lowest value for the intermediate nanocrystalline state. The charge transport in the glass is characterized by an intermediate value of E_σ, while the highest activation energy is observed for the polycrystal. One can assume that noticeable differences in E_σ values reflect distinct potential energy reliefs and diverse heights of the potential barriers in which thermally activated charge carriers overcome in the glass, nanocrystalline state and polycrystal. One may note that, in comparison with the data in [20], the E_σ values for the nanocrystalline state and polycrystal (Table 6.1) were determined from much broader temperature intervals in this work and, hence, can be assumed to be more accurate.

In accord with [18, 20], the increase of the conductivity between T_1 and T_2 (Fig. 6.3) can be attributed to a presence of nanometer-sized crystal nuclei in the intermediate state. Complete crystallization occurs through a formation of micrometer-sized crystallites (Fig. 6.2), resulting in a sharp and irreversible decrease of σ in the polycrystal. The above-described temperature cycling shows that the glass and the intermediate state were quite stable, and electrical properties did not change at temperatures below the glass transition point T_g. Hence, thermal treatment allows one to prepare highly dispersed intermediate states with increased conductivity, and such states can be stabilized by sufficiently fast cooling to temperatures well below T_g. It should be noted that nonstoichiometric Li_2O-$11.5GeO_2$ glass could be devitrified in a similar manner [18].

6.3.3 Complex Impedance Spectra

For the glass, intermediate nano- and polycrystalline states of Li_2O-$7GeO_2$ we studied spectra of the complex impedance $\rho^*(\omega)$. The samples were prepared by heating to certain temperatures in accord with the regimes described in Sec. 6.3.1. The measurements were carried out in the frequency range of 10^1–2×10^5 Hz and in the temperature interval up to 700 K, i.e. well below T_g, in order to keep the state of samples unchanged during the measurements.

Figure 6.4 shows the experimental data. One can see that for glass and polycrystal, the hodographs (Fig. 6.4a, c) consist of single arcs. Within the equivalent circuit approach [22], such hodographs can be described by the impedance of a parallel *RC* circuit. The centers of the arcs shift slightly downward on the abscissa ρ' axis, which is typical for real systems owing to a distribution of relaxation times $\tau = RC$. Usually such deviation is described by replacing the ordinary capacitance by a generalized frequency-dependent one, $C_n^* = B \cdot (i\omega)^{n-1}$ (ω – cyclic frequency, $0 \leq n \leq 1$) in the expression for the impedance of the parallel *RC* circuit:

$$\rho^*(\omega) = (S/l) \cdot \left(R^{-1} + B(i\omega)^n\right)^{-1}, \tag{6.2}$$

where S is the area of the electrodes and l the thickness of the sample.

Hodographs for the nanocrystalline state (Fig. 6.4b) differ from the diagrams for glass and polycrystal (Fig. 6.4a–c) and consist of two arcs. Such spectra can be simulated by the impedance of two serially connected parallel RC^* circuits:

$$\rho^*(\omega) = (S/l) \cdot \left(\frac{1}{R_1^{-1} + B_1 (i\omega)^{n_1}} + \frac{1}{R_2^{-1} + B_2 (i\omega)^{n_2}} \right). \tag{6.3}$$

Two arcs in the hodographs in Fig. 6.4b can be attributed to the coexistence of the nanometer-sized nuclei and the amorphous internuclei medium in the intermediate state. In previous works [18, 20], it was argued that the increased conductivity

of the nanocrystalline state results from its high dispersity. Accordingly, the high-frequency arc in the hodographs of Fig. 6.4b can be attributed to Li^+ ion motion within the crystalline nuclei, while the low-frequency arc corresponds to charge transport within the amorphous internuclei regions. One may note that the hodographs for the nanocrystalline state of nonstoichiometric Li_2O-11.5GeO_2 composition consist of only a single arc [23]. We assume that such discrepancy reflects different distributions of Li ions in the nanocrystalline states of stoichiometric (Li_2O-7GeO_2) and nonstoichiometric (Li_2O-11.5GeO_2) compositions, the latter of which contains an excess of GeO_2. The comparative analysis of the hodographs for Li_2O-7GeO_2 and Li_2O-11.5GeO_2 will be presented elsewhere soon.

Figure 6.5 shows an Arrhenius plot of the impedance relaxation rates $\tau^{-1}(1/T)$ for the glass and nanocrystalline state of Li_2O-7GeO_2. For the latter sample, we plot the relaxation rates τ^{-1} of both the high-frequency arc, which is assumed to reflect the charge transfer within ordered nuclei, and the low-frequency arc attributed to charge carrier motion within the embedding amorphous medium. The data for the polycrystal are omitted because of a low accuracy of τ^{-1} determination (see Fig.6.4c). Assuming that τ^{-1} can be related to the hopping rate of the charge carriers, one can conclude that the conductivity of the nanocrystalline state increases due to high Li^+ ion mobility within the nanometer-sized nuclei.

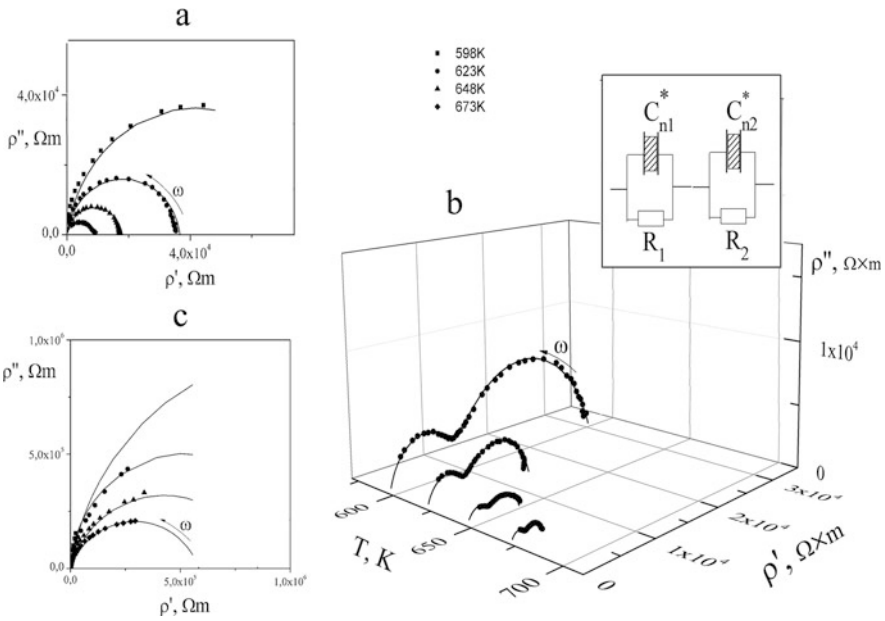

Fig. 6.4 Impedance spectra $\rho^*(\omega,T)$ for Li_2O-7GeO_2: (**a**) glass, (**b**) nanocrystalline state, and (**c**) polycrystal. Symbols represent the experimental data; solid lines are calculated by using Eqs. 6.2 and 6.3. The insert of panel (**b**) shows the equivalent circuit used to simulate the impedance of the nanocrystalline state

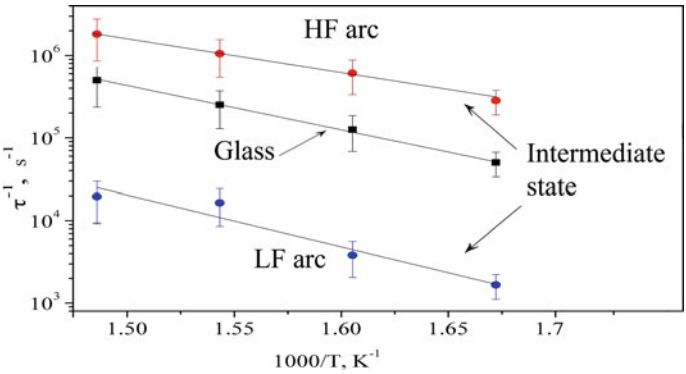

Fig. 6.5 Impedance relaxation rate τ^{-1} vs. $1/T$ for Li_2O-7GeO_2 states. For the nanocrystalline intermediate state, τ^{-1} is plotted for the high-frequency (HF) arc and the low-frequency (LF) arc

6.3.4 NMR Spin-Lattice Relaxation of ^{7}Li Isotope Nuclei

Measurements of ^{7}Li NMR SLR rates $T_1{}^{-1}$ provide information about local dynamics of Li^+ ions [24, 25]. Within the continuous diffusion model [24–30], the SLR rate $T_1{}^{-1}$ can be related to the correlation time τ_C describing the mean lifetime of the ions in some fixed positions. In the simplest case, which requires, e.g. the existence of an exponential correlation function of ion dynamics, the SLR rate $T_1{}^{-1}$ is given by

$$T_1{}^{-1}(\omega_L, T) \sim \begin{cases} \tau_C(T), & \text{if } (\omega_L \tau_C << 1), \\ \frac{1}{(\omega_L)^2}(\tau_C(T))^{-1}, & \text{if } (\omega_L \tau_C >> 1), \end{cases} \tag{6.4}$$

where $\omega_L \tau_C >> 1$ is fulfilled in the low-temperature interval (slow motion limit) and $\omega_L \tau_C << 1$ is valid in the high-temperature regime (fast motion limit). Motivated by the findings of the above conductivity and impedance studies, we assume in the following analysis that the correlation time obeys an Arrhenius law, $\tau_C(T) = \tau_0 \exp(E_{SLR}/k_B T)$.

The temperature-dependent ^{7}Li SLR rates $T_1{}^{-1}$ of the Li_2O-7GeO_2 glass, nanocrystalline state and polycrystal are plotted in Fig. 6.6. One can see that $T_1{}^{-1}$ increases when the temperature is increased for all Li_2O-7GeO_2 states. According to Eq. 6.4, this means that the slow motion limit applies and $T_1{}^{-1}$ is inversely proportional to the correlation time τ_C.

Comparing the data in Fig. 6.6, we observe that the intermediate nanocrystalline state has the highest SLR rate $T_1{}^{-1}$ and, hence, the fastest ion dynamics, followed by the glass and, finally, the polycrystal with the lowest SLR rate and slowest Li^+ motion. These findings are in qualitative agreement with the results of our impedance studies (Figs. 6.4 and 6.5). The SLR and impedance relaxations are fastest for the nanocrystalline state and slowest for polycrystalline state. These

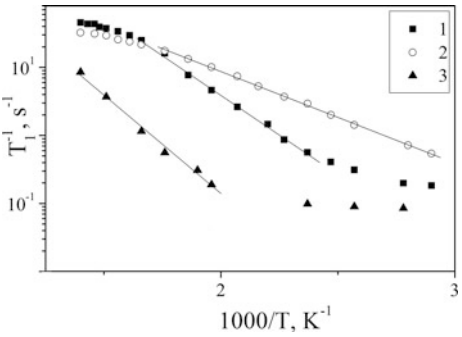

Fig. 6.6 ^{7}Li SLR rate $T_1{}^{-1}$ vs. $1/T$ for Li_2O-$7GeO_2$: (1) glass, (2) intermediate nanocrystalline state, and (3) polycrystal

observations indicate that the increased conductivity of the nanocrystalline state is due to a high mobility of Li^+ ions.

Activation energies E_{SLR}, determined from the SLR data, are added to Table 6.1 for comparison. One can see that for all states studied, the E_{SLR} values are appreciably smaller than the E_σ values. A similar discrepancy is observed for many other compounds [24, 25]. Such difference is actually expected when the correlation function of ion dynamics is not exponential, a situation met also for the present samples, as implied by the results of the above impedance studies. Then, the temperature dependence of $T_1{}^{-1}$ in the slow motion limit reflects not only the slowdown of the ion dynamics but also the stretching of the correlation loss, leading to a weaker increase upon cooling [24, 25]. As a consequence, E_{SLR} is smaller than E_σ under such circumstances. Despite these effects, both methods yield the same order of activation energies for the studied Li_2O-$7GeO_2$ states. The highest activation energy is found for the polycrystalline state, followed by the values for the glass, and the lowest activation energy is obtained for the nanocrystalline state.

Like impedance measurements, SLR analysis provides evidence for a hopping motion of Li^+ ions and allows us to link the enhanced conductivity of the nanocrystalline state with a high mobility of these charge carriers. This in turn can be attributed to a high dispersion of the intermediate state with nanometer-sized crystal nuclei, as indicated by our AFM studies. The transformation of the nanometer nuclei to micrometer crystallites upon formation of the polycrystalline state is accompanied by a sharp decrease of conductivity.

6.4 Conclusions

The electrical conductivity was measured during Li_2O-$7GeO_2$ glass crystallization upon heating. It was shown that heat treatment of Li_2O-$7GeO_2$ glass enabled to obtain a nanocrystalline state with increased electrical conductivity. Such nanocrystalline state could be stabilized by sufficiently fast cooling to temperatures below the glass transition point T_g. Complete glass crystallization happened through

transformation of nanometer-sized nuclei into micrometer-sized crystallites. It was accompanied by a sharp decrease of conductivity. Charge transport in the studied Li_2O-7GeO_2 states can be attributed to Li^+ ions that are mobile due to weak bonds to the germanium-oxygen structural framework.

Impedance spectra were recorded for glass, nanocrystalline and polycrystalline samples. Charge transport within the crystalline nuclei and their amorphous surroundings were distinguished for the nanocrystalline state. It was observed that the corresponding relaxation rates differ by about two orders of magnitude.

Measurements of ^{7}Li NMR SLR rates confirmed that the charge transport in the studied Li_2O-7GeO_2 compounds results from Li^+ ion motion. It was shown that the SLR rate and the impedance relaxation rate are highest and, hence, the ionic jumps are fastest in the nanocrystalline state. We conclude that the increase of the conductivity in the nanocrystalline state is caused by a high mobility of the Li^+ ions within nanometer-sized nuclei.

References

1. Maier J (2004) Ionic transport in nano-sized systems. J Solid State Ionics 175:7–12. https://doi.org/10.1016/j.ssi.2004.09.051
2. Maier J (2005) Nanoionics: ion transport and electrochemical storage in confined systems. J Nat Mater 4(11):805–815. https://doi.org/10.1038/nmat1513
3. Murthy MK (1964) Studies in germanium oxide systems: I, phase equilibria in the system Li_2O–GeO_2. J Am Ceram Soc 47(7):328–331. https://doi.org/10.1111/j.1151-2916.1964.tb14433.x
4. Haussuhl S, Wallrafen F, Recker K, Eckstein J (1980) Growth, elastic properties and phase transition of orthorhombic $Li_2Ge_7O_{15}$. Z Kristallogr 153:329–337
5. Vollenke H, Wittman A, Nowotny H (1970) Die kristall-structure des lithiumhepttagermanats $Li_2Ge_7O_{15}$. Monatch Chem 101:46–45
6. Iwata Y, Shibuya I, Wada M, Sawada A, Ishibashi Y (1987) Neutron diffraction study of structural phase transition in ferroelectric $Li_2Ge_7O_{15}$. J Phys Soc Jpn 56(7):2420–2427. https://doi.org/10.1143/JPSJ.56.2420
7. Ilyushin GD, Dem'yanets LN (2000) Crystal chemistry of germanates: characteristic structural features of Li, Ge-germanates. Crystallography Rep 45(4):626–632. https://doi.org/10.1134/1.1306574
8. Liebert BE, Huggins RA (1976) Ionic conductivity of Li_4GeO_4, Li_2GeO_3 and $Li_2Ge_7O_{15}$. Mat Res Bull 11(5):533–538. https://doi.org/10.1016/0025-5408(76)90235-X
9. Volnyanskii MD, Trubitsyn MP, Obaidat YAH (2008) Anisotropy of the electrical conductivity of lithium heptagermanate crystals. Phys Solid State 50(3):422–424. https://doi.org/10.1134/S1063783408030049
10. Trubitsyn MP, Volnyanskii MD, Obaidat YAH (2008) Ionic conduction in $Li_2Ge_7O_{15}$ crystals doped with Cr and Mn ions. Phys Solid State 50(7):1234–1237. https://doi.org/10.1134/S106378340807007X
11. Volnyanskii MD, Plyaka SN, Trubitsyn MP, Obaidat YAH (2012) Ion conduction and space-charge polarization processes in $Li_2Ge_7O_{15}$ crystals. Phys Solid State 54(3):499–503. https://doi.org/10.1134/S1063783412030353
12. Volnianskii M, Plyaka S, Trubitsyn M, Obaidat Y (2014) Frequency dispersion of conductivity and complex impedance in $Li_2Ge_7O_{15}$ single crystal. Ferroelectrics 462(1):74–79. https://doi.org/10.1080/00150193.2014.890880

13. Pernice P, Aronne A, Marotta M (1992) The non-isothermal devitrification of lithium tetragermanate glass. Mater Chem Phys 30(3):195–198. https://doi.org/10.1016/0254-0584(92)90223-u
14. Pernice P, Aronne A, Marotta M (1992) Crystallizing phases and kinetics of crystal growth in Li_2O-$_{19}GeO_2$ glass. J Mater Sci Lett 11:427–429
15. Marotta A, Pernice P, Aronne A, Catauro M (1993) The non-isothermal devitrification of lithium germanate glasses. J Ther Anal 40(1):181–188. https://doi.org/10.1007/BF02546568
16. Aronne A, Catauro M, Pernice P, Marotta A (1993) Gel synthesis and crystallization of Li_2O - $7GeO_2$ glass powders. Thermochim Acta 216:169–176
17. Volnyanskii MD, Nesterov AA, Trubitsyn MP (2012) Thermal and electrical properties of glass-ceramics based on lithium heptagermanate. Phys Solid State 54(5):945–946. https://doi.org/10.1134/S1063783412050459
18. Nesterov OO, Trubitsyn MP, Volnyanskii DM (2015) Metastable state of the Li_2O–$11.5GeO_2$ glass ceramics with a high electrical conductivity. Phys Solid State 57(4):683–688. https://doi.org/10.1134/S1063783415040204
19. Volnianskii MD, Nesterov OO, Trubitsyn MP (2014) Devitrification of the Li_2O – $x(GeO_2)$ glass. Ferroelectrics 466(1):126–130. https://doi.org/10.1080/00150193.2014.895173
20. Nesterov OO, Trubitsyn MP, Nedilko SG, Volnianskii MD, Plyaka SM, Rybak YO (2018) Ionic conductivity in multiphase Li_2O-$7GeO_2$ compounds. Acta Phys Polonica 133(4):892–896. https://doi.org/10.12693/APhysPolA.133.892
21. Gabriel J, Petrov OV, Kim Y, Martin SW, Vogel M (2015) Lithium ion dynamics in Li_2S+GeS_2+GeO_2 glasses studied using ^{7}Li NMR field-cycling relaxometry and line-shape analysis. Solid State Nucl Magn Reson 70:53–62. https://doi.org/10.1016/j.ssnmr.2015.06.004
22. Barsoukov E, Macdonald JR (2005) Impedance spectroscopy. Theory, experiment and applications, 2nd edn. Wiley, New York, p 616. ISBN: 978-0-471-64749-2
23. Nesterov OO, Trubitsyn MP, Plyaka SM, Volnyanskii DM (2015) Complex impedance spectra of glass and glass ceramic Li_2O–$11.5GeO_2$. Phys Solid State 57(9):1759–1763. https://doi.org/10.1134/S1063783415090255
24. Böhmer R, Jeffrey KR, Vogel M (2007) Solid-state Li NMR with applications to the translational dynamics in ion conductors. Prog Nucl Magn Reson Spectrosc 50(2–3):87–174. https://doi.org/10.1016/j.pnmrs.2006.12.001
25. Böhmer R, Storek M, Vogel M (2018) NMR studies of ionic dynamics. In: Hodgkinson P (ed) Modern methods in solid-state NMR: a practitioners guide, vol 7. Royal Society of Chemistry, pp 193–230. https://doi.org/10.1039/9781788010467-00193
26. Torrey HC (1953) Nuclear spin relaxation by translational diffusion. Phys Rev 92(4):962–969. https://doi.org/10.1103/physrev.92.962
27. Kimmich R, Voigt G (1978) Zeitschrift fur Naturforschung. Astrophysik. Physik und Physikalische Chemie 3BA:1294–1306
28. Deutch JM (1972) J Chem Phys 56:6076–6081
29. Avogadro A, Villa M (1977) Nuclear magnetic resonance in a two dimensional system. J Chem Phys 66(6):2359–2367. https://doi.org/10.1063/1.434272
30. Bjorkstam JL, Villa M (1980) Second-order quadrupolar and low-dimensionality effects upon NMR resonance spectra. Phys Rev B 22(11):5025–5032. https://doi.org/10.1103/physrevb.22.5025